Electrochemical and Surface Studies of Thiourea-formaldehyde as corrosion Inhibitor for N80 Steel in Chloride Media

Hongqiang Wan[1,], Peiying Han[1], Shuai Ge[1], Fancong Li[1], Simiao Zhang[1], Huan Li[1], Ambrish Singh[2]*

[1] Mechanical and Electrical Engineering Institute, Xian Technological University, Shaanxi, China.
[2] School of Materials and Engineering(Southwest Petroleum University), Chengdu, 610500, PR China.
[*]E-mail: hongqiangwang2000@hotmail.com, hongqiangwang@aliyun.com

Effective Thiourea formaldehyde (TF) inhibitor was synthesized and used for the corrosion mitigation of N80 steel in 3.5% NaCl solution containing CO_2. The electrochemical impedance spectroscopy (EIS) and Tafel polarization were investigated to evaluate the inhibition efficiency of the inhibitor. Surface studies including Fourier transform infrared (FTIR) spectroscopy, scanning electrochemical microscopy (SECM), atomic force microscopy (AFM) and scanning electron microscopy (SEM) techniques were performed to get a clear picture of the metal-inhibitor mechanism and to compare the surface condition with and without inhibitor. Theoretical computations were evaluated to support the experimental results. The impedance figures showed the increase in diameter in presence of inhibitor thereby increasing efficiency. Shift towards anodic and cathodic regions suggested that the TF inhibitor belongs to mixed type category. Scanning electrochemical microscopy (SECM) revealed the action of protection by inhibitor acting as an insulator. The surface analysis through AFM and SEM for N80 specimens showed the smooth surface in existence of inhibitor than in its absence. Theoretical parameters also well supported the results from other techniques.

1. INTRODUCTION

Steel corrosion is very common is oil industries and refineries. N80 steel is widely used due to its cost effectiveness and availability. N80 steel is basically used as a casing pipe, drilling pipe in oil rigs, and tubing's for transportation of oil. Production of oil is an important process in petroleum industry that can be improved by different techniques such as enhanced oil recovery, stimulation of well, flooding of reservoir and use of acids. Presence of carbon dioxide in the reservoirs can be very dangerous as it can react with NaCl and form carbonic acid which can further give rise to various

forms of steel corrosion. To mitigate steel corrosion inhibitors are used which is one of the oldest and most common methods [1].

The presence of electron donating heteroatoms is a boon to the inhibitor structure. These heteroatoms (N, O, S and P donor groups) can participate in complex formation with the metal surface. The complex/film forming process can occur through chemical or physical adsorption process. The complex can act as an obstacle to split the metal from the caustic media. The presence of ample heteroatoms in our current Thiourea formaldehyde compound was the motivation to synthesize and test it as potential inhibitor. Formaldehyde based resins have various applications in several industries due to their better efficiency and durability [2].

In the present work the mitigating effect of Thiourea Formaldehyde (TF) was examined on the corrosion of N80 steel in sweet corrosive media using Tafel polarization and electrochemical impedance spectroscopy (EIS) methods. The N80 steel surface was inspected through Fourier transform infrared (FTIR) spectroscopy, scanning electrochemical microscopy (SECM), atomic force microscopy (AFM) and scanning electron microscopy (SEM) techniques [3].

2. EXPERIMENTAL OBSERVATIONS

2.1. Synthesis of Thiourea Formaldehyde (TF)

The inhibitor used in the current study was synthesized according to the experimental process described earlier [4]. Figure 1 represents the molecular configuration of Thiourea Formaldehyde compound (TF). All the electrochemical tests were performed on N80 steel samples of composition (wt.%): C 0.31; Si 0.19; Mn 0.92; P 0.010; S 0.008; Cr 0.2; Fe balance. The samples were abraded as directed in ASTM A262 with emery paper of different size. The samples were washed with alcohol, left to dry and then kept in desiccator to remove humidity. The samples of size 30 mm × 3 mm × 3 mmwere used for the impedance and Tafel polarization studies. Sodium chloride of high quality purchased from authentic chemical shop was used to prepare the corrosive solution of 3.5% NaCl with distilled water. Carbon dioxide was purged into the solution for 1 hour at 10 MPa till the pH of 4.8 was attained. The cell was then preserved with epoxy resin to uphold the same test environment. Blank solution used is 3.5% NaCl without inhibitor. Inhibitor solutions are 3.5% NaCl with different concentrations of TF inhibitor.
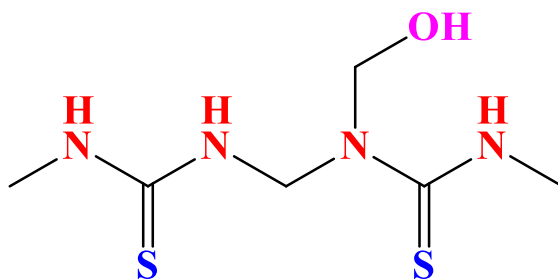
Figure 1. Chemical structure of thiourea-formaldehyde (TF).

2.2. Fourier Transform Infrared Spectroscopy (FTIR)

Reflectance mode of Nicolet-6700 spectrophotometer was utilized to trace FT-IR peaks of the TF on the N80 metal surface [5]. The peaks as obtained are shown in Figure 2 representing different vibrating and stretching frequencies. Some of the important peaks represents 955.02 cm^{-1} -OH group/ olefin's single substitution; 1129.24 cm^{-1} C-O stretching; 1270.27 cm^{-1} C=C (Aromatic)/ C-O stretching; 1398.86 cm^{-1} C=C (Aromatic) / N-H stretching; 1635.29 cm^{-1} C=O stretching; 2900.43 cm^{-1} –CH stretching vibration; 2975.09 cm^{-1} –CH stretching/ OH group; 3410.63 cm^{-1} N-H stretching.

2.3. Electrochemical measurements

A four neck cell assembly was used to run all the electrochemical tests using an Autolab workstation under static conditions. A reference, auxiliary and working electrode were used in the cell assembly. An immersion period of 30 minutes was employed before the test to attain a stable potential. Impedance computations were performed in a frequency array from 100 kHz to 0.00001 kHz [6].

Potentiodynamic Tafel figures were acquired by transforming the potential from −300 to +300 mV at a scan rate of 1 mV s^{-1}. The anodic and cathodic curves of the Tafel were examined and plotted to obtain the values of corrosion current densities (I_{corr}) [7]. The equation mentioned below was utilized to evaluate the inhibition efficiency from the obtained I_{corr} values:

$$\eta\% = \frac{I_{corr}^0 - I_{corr}^{'}}{I_{corr}^0} \times 100 \qquad (1)$$

where, I_{corr}^0 and $I_{corr}^{'}$ be the corrosion currents in lack and in the existence of an inhibitor, correspondingly. The diameter of the Nyquist curves gave the values of charge transfer resistance (R_{ct}) after fitting the equivalent circuit. The equation below was used to evaluate the inhibition efficiency from the R_{ct} values:

$$\eta\% = \frac{R_{ct}^{'} - R_{ct}^0}{R_{ct}^{'}} \times 100 \qquad (2)$$

where, $R_{ct}^{'}$ and R_{ct}^0 are the charge transfer resistance in occurrence and in the deficiency of an inhibitor, correspondingly.

2.4. Scanning Electrochemical Microscopy

Bard and co-workers developed SECM in 1989 to detect the micro electrochemical changes at the metal surface [8]. This technique can detect the uniform corrosion as well as can give influential information about the localised corrosion. The technique is very versatile and comes with varied options of research modes to be selected depending on the metal-solution metal-probe behaviour [9, 10].

The metal samples of size 30 × 3 × 3 mm were used to perform all the tests. An electrochemical workstation of CHI was used with a 10 μm platinum tip as the probe. The assembly of

electrochemical cell was similar as utilized in the traditional electrochemical tests having working, auxiliary and referenceelectrode. The size of all the electrodes was very small as compared to the electrodes used on Autolab electrochemical workstation due to which the micro level changes can be monitored. The distance of the probe from metal surface was kept at ~ 10 μm for all the tests at a scam rate of 80 μm/step [11].

2.5. Scanning Electron Microscopy

The changes on the metal surface in lack and in presence of inhibitor were explored through SEM. Prior to the test the metal samples were engrossed in the corrosive solution with and without inhibitor. The samples were washed with alcohol to remove any salt or by-products on the surface. The samples were then dehydrated at room temperature and set aside in desiccator. TESCAN VEGA and Zeiss were used to record the morphological changes on the metal surface after being exposed to the corrosive media [12].

2.6 Atomic Force Microscopy

The N80 metal samples were immersed in the corrosive solution before being exposed to the AFM test. The metal sample was then sanitized with water, washed with alcohol and dried carefully. AFM tests were performed using a NT-MDT multimode AFM workstation [13].

2.7 Theoretical Calculations

Theoretical calculations can provide data that can predict the reactivity of a particular molecule. Density functional theory (DFT) module is used in Gaussian software to get the values of the reactive sites. All calculations were carried out using DFT/B3LYP methods using 6-311G (d, p) basis set to predict the highest occupied molecular orbital (E_{HOMO}) and lowest unoccupied molecular orbital (E_{LUMO}) and energy gap ($\Delta E = E_{LUMO} - E_{HOMO}$) values.

3. RESULTS AND DISCUSSION

3.1. EIS Measurement

Electrochemical impedance approach is helpful to find the capacitive and resistive change at the metal solution boundary, which assist to recognize the corrosion mitigationability of the TF molecules. Figure2a depicts the impedance graph of N80 steel in the absence and presence of different concentration of TF in corrosive solution. The Nyquist curves of solution without inhibitor consist of only one capacitive loop at the higher frequency region.Though, adding up of the TF inhibitor causes the variation in the diameter of the Nyquist graphs which shows a depressed semicircle at higher

frequency and an inductive loop at the lower frequency region. This phenomenon is known as dispersion of frequency due to roughness and other irregularities of solid surface and is often associated with metal electrodes. The inductive loop occurred due to the steel dissolution during the adsorption process taking place or due to the presence of the by-products on the electrode surface [14-16]. For 25 ppm inhibitor concentration and 50 ppm inhibitor concentration an inductive loop is observed which is absent for 100 ppm concentration which may be due to the number of exposed active centres for steel dissolution.

The impedance spectra for corrosive solution were evaluatedby using the equivalent circuit to fit the tests outcome (Figure 2b) that was used before to elucidate the corrosion process at interface [17, 18]. The circuit contains R_s as the solution resistance, R_{ct} as the charge transfer resistance, Las inductance, and CPE as a constant phase element. To fit the curve more appropriately capacitance is replaced with CPE in the circuit [19].
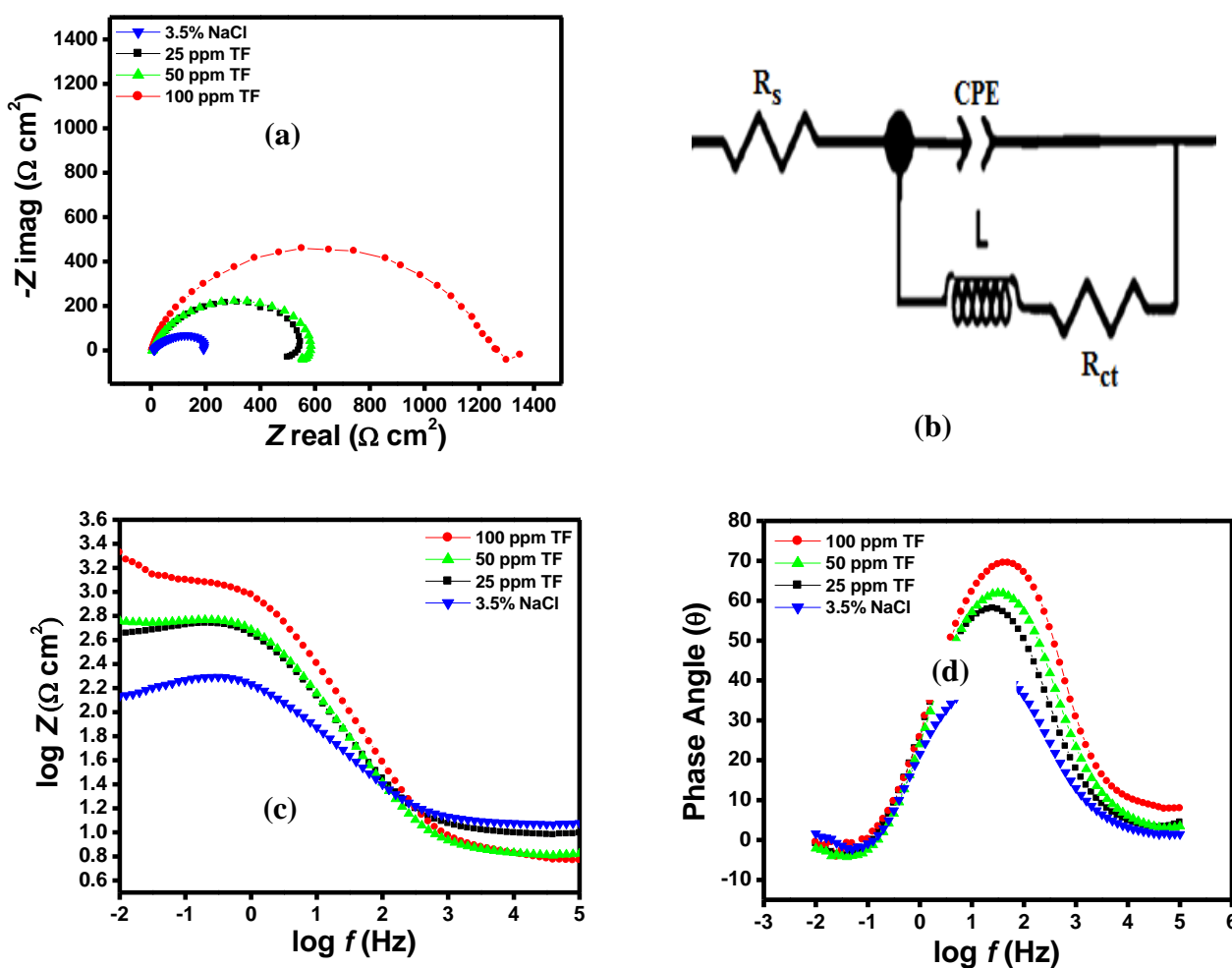
Figure 2. Electrochemical results of (a) Nyquist plot (b) Equivalent circuit (c) Bode plot and (d) Theta-frequency plots for N80 steel with and without TF.

The value of *n* represents the surface changes on the electrode surface.The lower value of*n* for solution without inhibitor (*n* = 0.728) point to a surface irregularity consequential from roughening of metal surface and/or due to corrosion products [20]. The higher value of *n* after the addition of inhibitor indicates that the surface is uniform and roughness is reduced due to the blockage of active adsorption sites on the metal surface [21]. The thickness of the inhibitor film on the metal surface is related to the capacitance according to the following Helmholtz model[22, 23]:

$$C_{\text{dl}} = \frac{\varepsilon\varepsilon_o}{d} S \tag{3}$$

where, ε_o be the permittivity of free space (8.854×10^{-12} F m^{-1}), εrepresents the local dielectric constant of the solution, *S* be the surface area of the electrode, and *d* be the thickness of the protective layer [24].

Table 1. Parameters obtained from Nyquist for N80 steel with and without TF.

Solution	R_s	R_{ct}	*n*	$Y\circ$	*L*	*Chi*	η	Surf. coverage
	(Ωcm^2)	(Ω cm^2)		(Ω^{-1}s^n/cm^2)	(Hcm^2)	Square	%	θ
3.5% NaCl	2.1	145	0.728	219	-	0.0006	-	-
TF 25 ppm	3.3	550	0.742	121	113	0.0018	74	0.74
TF 50 ppm	1.9	589	0.798	103	124	0.0015	75	0.75
TF100 ppm	2.4	1387	0.816	92	-	0.0009	90	0.90

The efficiency of the inhibitor increases with the increase in concentration as can be seen in Table 1. The increase in concentration led to a wide surface coverage by the inhibitor molecule thereby increasing the inhibition efficiency. As can be seen from Table 1 that the value of R_{ct} varies significantly after the addition of the inhibitor in the solution. This is also relevant to the Nyquist figure where the diameter increases with increase in inhibitor concentration without changing the overall mechanism. The maximum inhibition efficiency of 1387 Ω cm^2 is observed at 100 ppm in the corrosive solution [25].

Table 2. The slopes obtained from Bode plots (*S*) and the maximum phase angle (α) for N80 steel with and without TF.

C (ppm)	-*S*	-$\alpha°$
3.5% NaCl	0.489	36.4
TF 25 ppm	0.498	59.3
TF 50 ppm	0.512	62.8
TF 100 ppm	0.694	70.4

The Bode impedance and phase angle graphsplotted for N80 steel in 3.5% NaCl in absence and presence of TFis shown in Figure2c. It can be seen from the figure that the value increases in presence

of TF at lower frequency than in its absence. Table 2 shows the values of slope obtained from bode plots which shows an increase with concentration and tends towards unity (-1) which may be due to the adsorption of inhibitor molecules on the N80 steel surface and as a result protecting it from corrosion [26]. In addition, the values of phase angle increases (Figure2d)from -36.4° (3.5% NaCl with CO_2) to TF 25 ppm (-59.3°), TF 50 ppm (-62.8°), and TF 100 ppm (-70.4°) as shown in Table 2.This raise in the phase angle towards further negative values recommend the inhibitive characteristic of inhibitor molecules due to adsorption above the N80 steel surface [27].

3.2. Tafel Measurements

The kinetics of anodic and cathodic slopes in corrosive media on N80 steel was investigated by Tafel polarization technique. The acquired curves are depicted in Figure 3. Examination of graph discloses that the curves werealtered for both anodic and cathodic region. Moreover, the contour of the curves is alike in absence and presence of inhibitor which entail that the corrosion reaction mechanism is not modified by inhibitor addition. The analyzed data of the anodic and cathodic parameters are tabulated in Table 3 [28].
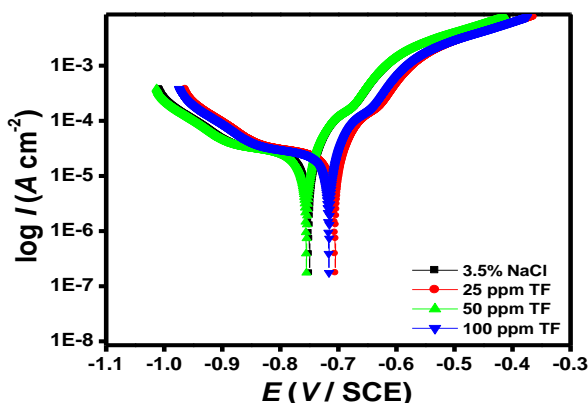
Figure 3. Tafel polarization plots for N80 steel in 3.5% NaCl solution with and without TF.

Table 3. Polarization parameters for N80 steel in 3.5% NaCl with and without TF.

						Tafel data	
Solution	E_{corr}	I_{corr}	b_a	$-b_c$	η	**Surface coverage**	
	(V vs. SCE)	**(mA cm^{-2})**	**(mV d^{-1})**	**(mV d^{-1})**	**(%)**	θ	
3.5% NaCl	-0.733	0.91	46	103	-	-	
TF 25 ppm	-0.722	0.21	58	92	77	0.77	
TF 50 ppm	-0.743	0.19	53	86	79	0.79	
TF 100 ppm	-0.718	0.08	67	89	91	0.91	

The careful assessment of table discloses that the corrosion current density (i_{corr}) in presence of inhibitor is quite less (0.08mA/cm^2 for TF at 100 ppm) that is contrast to the blank (0.91mA/cm^2) and

the maximum mitigation is 91% in case of TF 100 ppm as compare to blank, which suggest the formation of metal-TF complex at the interface due to adsorption [29]. The inhibitor molecules adsorbed on the metal protects it from the corrosive solution and thereby mitigates corrosion reaction [30]. According to previous research papers [31-33] (i) if E_{corr} shows a displacement >85 mV, the inhibitor can be categorized into cathodic or anodic (ii) if displacement in E_{corr} is <85, the inhibitor can be categorizedas mixed type. In the present study, shift in E_{corr} values is in the range of 25 mV, signifying that TF belong to mixed type category [34, 35].

3.3. Adsorption behavior of the inhibitor
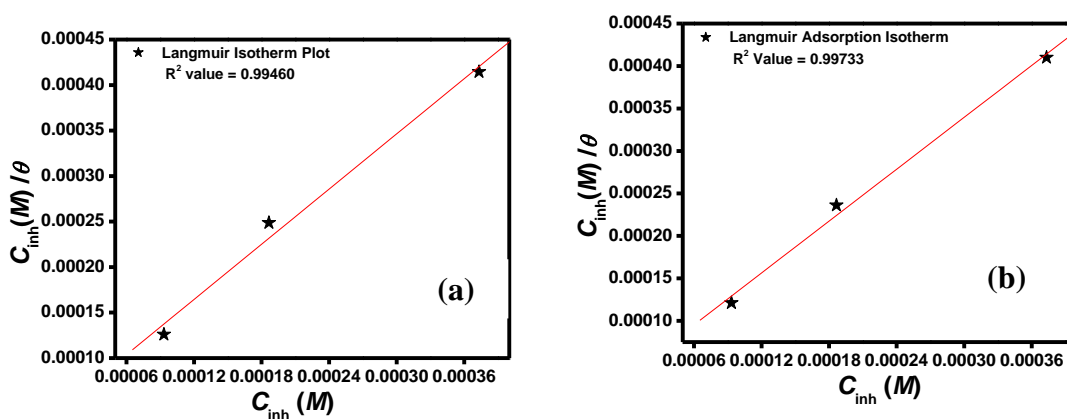
Figure 4. Langmuir isotherm plots for (a) EIS and (b) Tafel

Inhibitor can adsorb on to a metal surface depending on the behaviour of metal surface, temperature, electronic and steric effects. Chemical adsorption or physical adsorption could take place depending on the surface-interface activities. The penetration of water (corrosive media) on the metal surface causes corrosion. So, to develop a mechanism of action we consider the adsorption of water on the metal-solution interface. Therefore, this process can be recalled as a quasi-substitution procedure between the inhibitor in the aqueous phase $Inh_{(sol)}$ and water molecules at the electrode interface $H_2O_{(ads)}$ [36].

$$Inh_{(sol)} + xH_2O_{(ads)} \rightarrow Inh_{(ads)} + xH_2O_{(sol)} \tag{4}$$
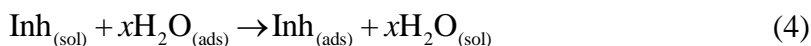
Where x represents the ratio at which water molecules are being replaced by one molecule of TF. Adsorption can endow with the basic knowledge about the interaction between TF and N80 steel surface. As a result, the surface coverage (θ) and concentration of TF (C_{inh}) have been used to establish the superlative isotherm from Langmuir, Temkin and Frendulich isotherms. The greatestoutcome was obtained for Langmuir isotherm as the fit was accurate and linear compared to other isotherms. The equation below was utilized to derive the plot for Langmuir isotherm [37].

$$\theta = \frac{K_{ads}C_{inh}}{1+K_{ads}C_{inh}} \qquad \text{(Langmuir isotherm)} \tag{5}$$

where, K_{ads} represents the constant for the adsorption or desorptionreaction. The equation can be rewritten as [38]:

$$\frac{C_{\text{inh}}}{\theta} = \frac{1}{K_{\text{ads}}} + C_{\text{inh}} \tag{6}$$

A linear graph was obtained with R^2 values close to unity using equation 6 as depicted in Figure 4a, and 4b. The straight line of the plot vindicated the best fit to Langmuir isotherm. The value of the correlation coefficient (R^2) obtained was in the range of 0.99460 for EIS and 0.99733 for Tafel polarization [39, 40]. According to the previous research done K_{ads} depicts the endurance between adsorbate and adsorbent. So, higher values of K_{ads} justify excellent adsorption of inhibitor on the metal surface [41]. K_{ads} and free energy of adsorption (ΔG_{ads}) can be used together as in the equation below:

$$\Delta G^{\circ}_{ads} = -RT \ln(55.5 K_{ads}) \tag{7}$$

where, the value 55.5 in mol L^{-1} is the concentration of water. Table 4 shows the values obtained for K_{ads} and $\Delta G^{\circ}_{\text{ads}}$. The spontaneity of a reaction depends on the negative values of $\Delta G^{\circ}_{\text{ads}}$ which further validate the stability of the adsorbed inhibitor film on the metal surface [42].

Table 4. Thermodynamic parameters for the adsorption of TF on N80 steel.

	EIS		Tafel	
Concentration	K_{ads}	$\Delta G^{\circ}_{\text{ads}}$	K_{ads}	$\Delta G^{\circ}_{\text{ads}}$
M	**M^{-1}**	**kJ mol^{-1}**	**M^{-1}**	**kJ mol^{-1}**
3.5% NaCl	-	-	-	-
100 ppm TF	24120	-34.9	27097	-35.2

Adsorption can of chemical or physical type depending on the values of $\Delta G^{\circ}_{\text{ads}}$. Values of $\Delta G^{\circ}_{\text{ads}} \leq -20$ kJ mol^{-1} signify physisorption, whereas value further than -40 kJ mol^{-1} relates chemisorption [43]. The calculated value of $\Delta G^{\circ}_{\text{ads}}$ for TF is in the range -34.9 kJ mol^{-1} to -35.2 kJ mol^{-1} (table 4), which indicates that TF inhibitor adsorbed onto the steel exterior both by physical and chemical adsorptions process [44, 45].

3.4. Scanning Electrochemical Microscopy

SECM is a new practice used worldwide to determine the localised and uniform corrosion on a metal surface. There are various modes of operation in SECM depending on the behavior and conditions of solution-metal interactions. SECM offers several advantages as it can equally operate on coated/films and non-coated metal samples and the results obtained can be used to relate the difference. In amperometry mode the probe is moved towards the metal sample in X, Y, and Z plane at a certain distance.
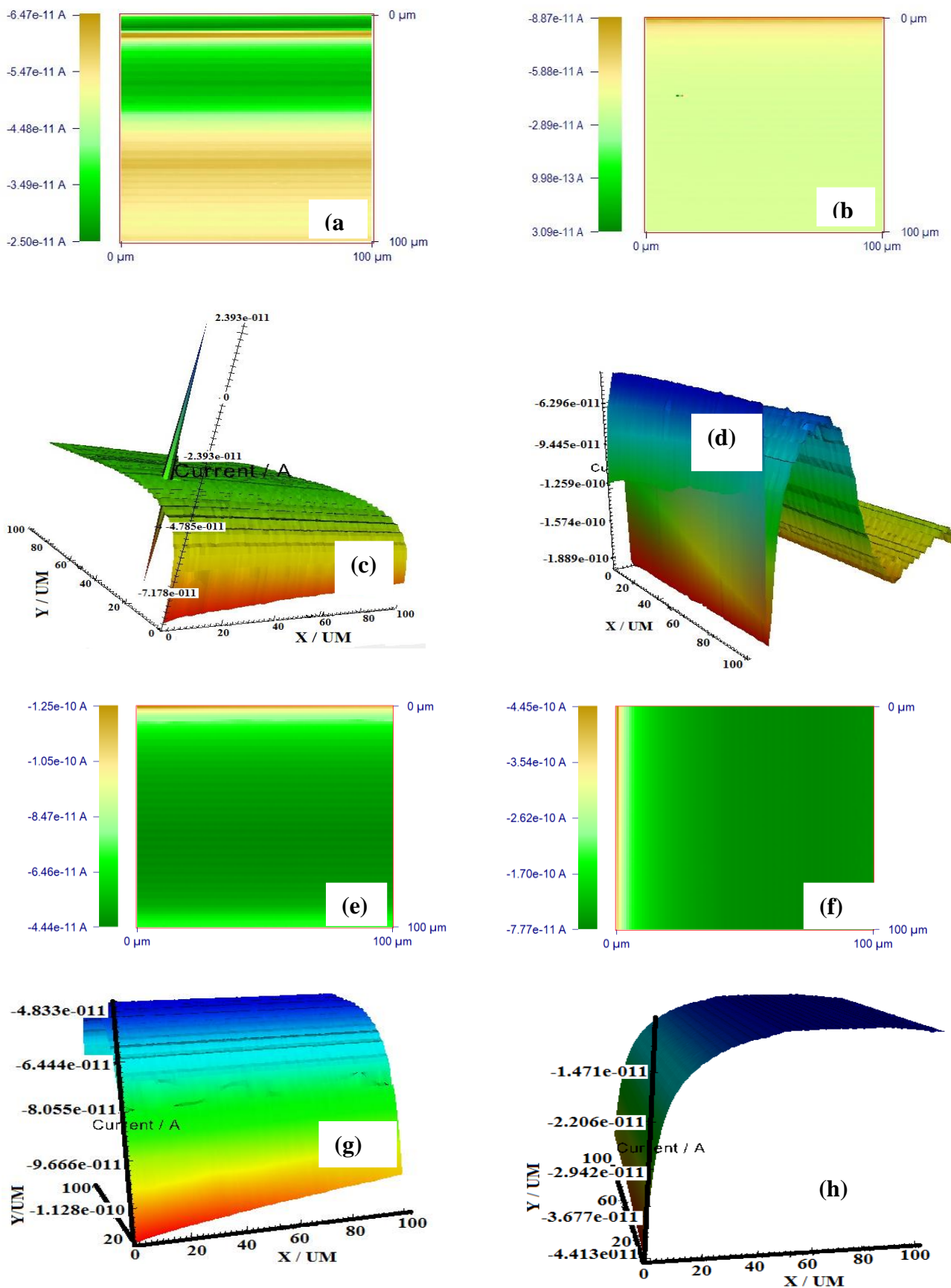
Figure 5. SECM images for (a) 3.5% NaCl *x* axis 2D (b) 3.5% NaCl *y* axis 2D (c) 3.5% NaCl *x* axis 3D (d) 3.5% NaCl *y* axis 3D (e) 100 ppm TF *x* axis 2D (f) 100 ppm TF *y* axis 2D (g) 100 ppm TF *x* axis 3D (h) 100 ppm TF *y* axis 3D.

Prior to the test the distance is maintained through probe approach curve option to set the same distance for all samples. This method provides a 2-D graph (colour map) and a 3-D graph for further evaluation of the surface as shown in Figure 5a-h [46-48].

As the probe is stimulated towards the metal exterior through solution the current is being recorded for metal surface with and without inhibitor. Figure 5a, 5b shows the colour map of x and y axis for the corrosive solution for N80 steel. Here, the distribution of current is very random and a high current can be observed on the steel surface represented by brownish colour. While Figure 5e and 5f shows uniform current distribution throughout the colour map with lower current for TF inhibitor than the corrosive solution. Figure 5c and 5d shows the 3-D figures for the corrosive solution and a higher current can be noticed as compare to Figure 5g and 5h where the current remains to be on the lower side. This phenomenon can be explained on the basis of conducting and insulating properties. As the probe come near to the metal surface without any inhibitor film on it a higher current is observed as the surface acts conducting and can pass currenteasily. On the other hand, when the probe approaches the metal surface with an inhibitor film on it the current tends to be lower drastically. This is due to the fact that the surface becomes insulating with an inhibitor film on it [49, 50].

3.5. Scanning Electron Microscopy

SEM photos with and without TF are shown in Figure 6a, 6b. A damaged and rough N80 steel surface can be seen in Figure 6a in absence of TF inhibitor. The corrosion of the metal surface led to cracks, pits and dents which are visible in the figure. Nonetheless, a smooth and less corroded surface was observed in Figure 6b for N80 steel surface in presence of TF inhibitor. The surface was less damaged without pits and cracks. This can be attributed to the good performance by TF inhibitor on N80 steel surface that blocked the corrosive media by forming a film/complex on the metal surface [51].
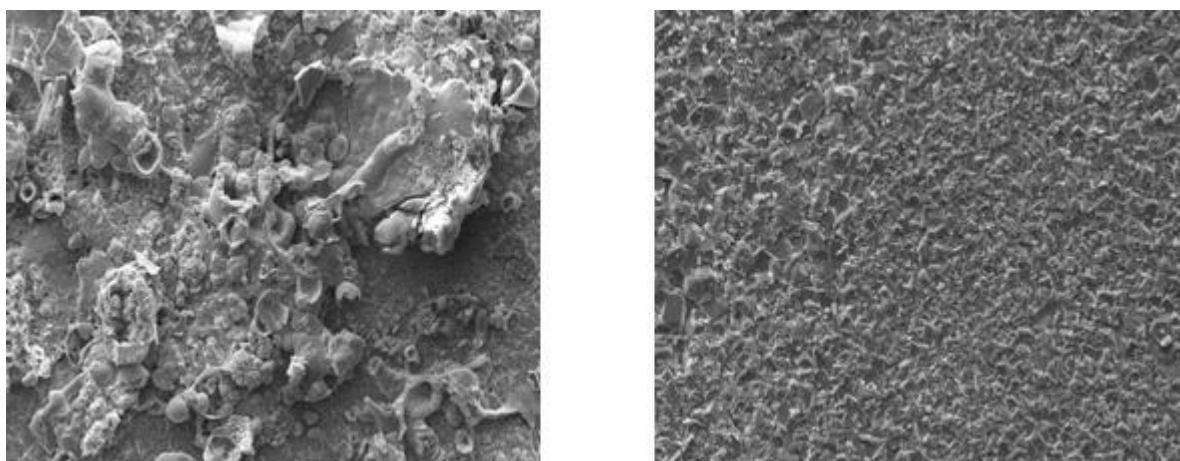
Figure 6. Photographs of SEM for (a) 3.5% NaCl solution and (b) 100 ppm TF.

3.6. Atomic Force Microscopy

The 3-D pictures of AFM with and without TF inhibitor is shown in Figure 7a, 7b. As can be seen from Figure 7a the metal surface is sturdily dented without TF inhibitor and the roughness level is very high. On the other hand, in charisma of TF inhibitor the roughness level is reduced and the surface appears to be smooth as shown in Figure 7b [52].
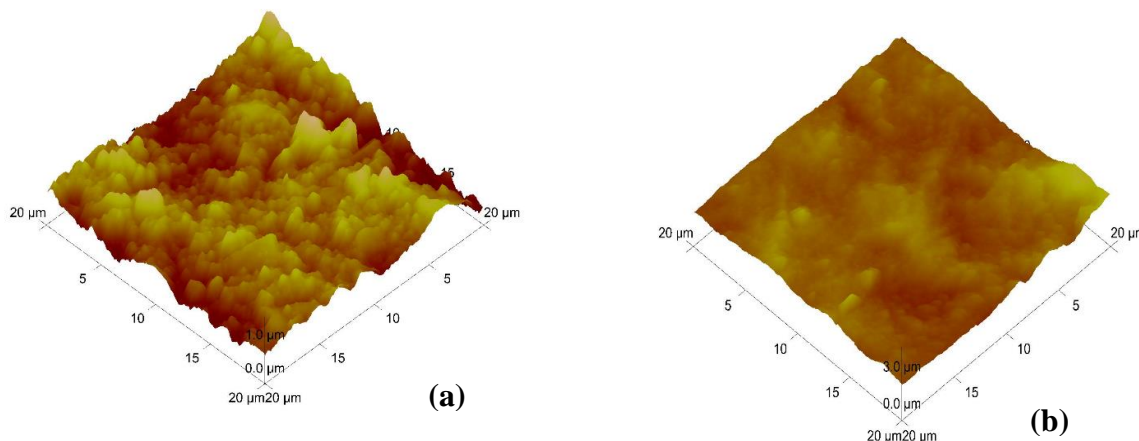
Figure 7.AFM images for (a) 3.5% NaCl solution and (b) 100 ppm TF.

3.7. Quantum Chemical Calculations
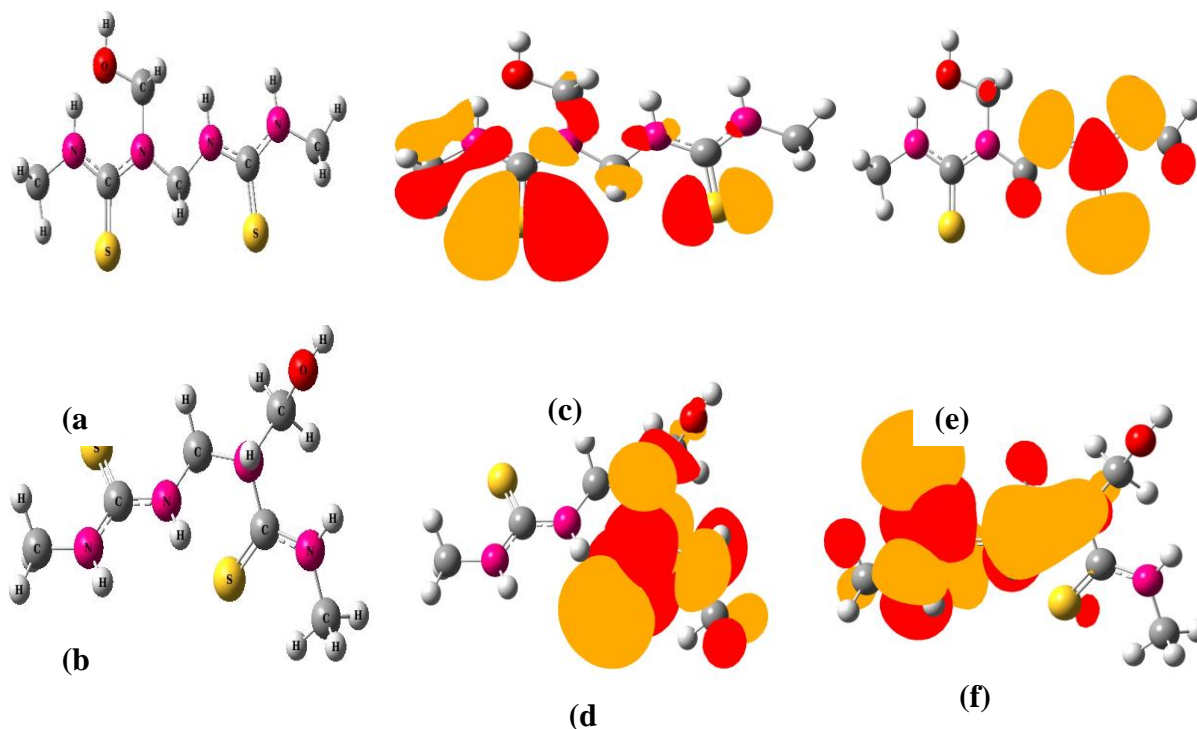
Figure 5.(a) neutral and (b) protonatedoptimized molecular structure, (c) HOMO-neutral and (d) HOMO-protonated, (e) LUMO-neutral and (f) LUMO-protonated frontier molecular orbital density distribution of TF inhibitor.

Quantum chemicalparameters for Ketoconazole such as E_{HOMO} (high occupied molecular orbital energy), E_{LUMO} (lowest unoccupied molecular orbital energy) and the dipole moment (μ) were calculated. The results are given in Table 4.

Table 4. Calculated quantum chemical parameters of studied TF inhibitor

Inhibitor	E_{HOMO}	E_{LUMO}	ΔE	EA	χ	ΔN
TF-neutral	-2.498048	-0.081056	2.416992	0.081056	1.289552	1.4606784
TF-protonated	-5.911104	-0.060656	5.850448	0.060656	2.98588	0.31350078

The protonated and neutral forms of TF inhibitor are represented in Figure 5.The protonated and neutral form depict the optimized structure, the highest occupied molecular orbital (HOMO), and the lowest unoccupied molecular orbital (LUMO) pictures. The data obtained from E_{HOMO} represents the electron donating ability of the TF molecules and data of E_{LUMO} represents the electron accepting tendency of the TF molecules. So, molecules with higher E_{HOMO} values are better electron donor to and molecules with the lower value of E_{LUMO} are good electron acceptors [53, 54]. The theoretical factors for both neutral and protonated TF moleculeare tabulated in Tables 4. A significant evaluator of the reactivity utility for the TF is the energy gap (ΔE) and it explains the adsorption capability of the TF molecule above the metal facade. Consequently, the adsorption and reactivity of the molecules will increase with lesser energy gap due to low ionization energy required for eliminating electron from the highest occupied energy point [55].

Additionally, it could be observed form table 4 that the E_{HOMO} values of protonated TF has lower values contrast to the neutral one. This suggests that the ability of the protonated TF to donate electron is less that neutral TF. The protonated TF showed a lower E_{LUMO} values suggesting a better capability to accept electron than neutral TF [56]. The calculated values of ΔN expose that all ΔN values in neutral TF is positive and so electron shift takes place from TF to metal surface. Consequently, the careful observation of Table 4 suggests that the protonated TF shows different results as compared to neutral TF [57]. So, protonation of molecule is an important aspect to compare the parameters as obtained from neutral molecules.

4. CONCLUSIONS

- TF can be an effective inhibitor in 3.5% NaCl media saturated with carbon dioxide. The efficiency was observed to increase with increase in concentration.

- Langmuir adsorption isotherm was the best fit with better regression coefficient value.

- TF acted as mixed type as indicated by the mixed cathodic and anodic shifts.

- The SECM, AFM and SEM analyses confirmed the mitigating action of TF molecule on the steel surface through effective adsorption

References

1. Ambrish Singh, K. R. Ansari, M. A. Quraishi, HassaneLgaz, Yuanhua Lin, *J. Alloys Comp.*, 762 (2018) 347.
2. M. A. Quraishi, D.Jamal, *Mater. Chem. Phys.*, 68 (2001) 283.
3. A. Singh, K. R. Ansari, X. Xu, Z. Sun, A. Kumar, Y.Lin, (2017) *Sci. Report.*, 7 (2017) DOI:10.1038/s41598-017-13877-0.
4. K.R. Ansari, M.A.Quraishi, A.Singh, *J. Ind. Eng. Chem.,* 25 (2015) 89.
5. A. Singh, K.R. Ansari, A. Kumar, W. Liu, C.Songsong, Y. Lin, *J. Alloys Comp.,*712 (2017)121.
6. B.Evgenij, J. R. Macdonald, Impedance Spectroscopy Theory, Experiment, and Applications, John Wiley & Sons, New Jersey, (2005).
7. A. Singh, K.R. Ansari, J. Haque, P. Dohare, H. Lgaz, R. Salghi, M.A.Quraishi, *J. Taiwan Inst. Chem. E.,* 82 (2018) 233.
8. F. R. F. Fan, J.Kwak, O. Lev, *Analyt. Chem.,*61 (1989) 132.
9. A. J. Bard, G.Denuault, C. Lee, D.Mandler, D. O.Wipf, *Acc. Chem. Res.*, 23 (1990) 357-363.
10. C. Lee, A. J. Bard, *Analyt. Chem.,*62 (1990) 1906 .
11. A. Singh, Y. Lin, E. E. Ebenso, W. Liu, B. Huang, *Int. J. Electrochem. Sci.*, 9 (2014) 5993.
12. A. Singh, E. E. Ebenso, M. A. Quraishi, Y. Lin, *Int. J. Electrochem. Sci.*, 9 (2014) 7495.
13. A. Singh, Y. Lin, Eno. E. Ebenso, W. Liu, D. Kuanhai, J. Pan, B. Huang, *Int. J. Electrochem. Sci.,* 9 (2014) 5585.
14. A. Singh, Y. Lin, W.Liu, S. Yu, J.Pan, C. Ren, D. Kuanhai, *J. Ind. Eng. Chem.*, 20 (2014) 4276.
15. I.Ahamad, R. Prasad, M. A.Quraishi, *Corros. Sci.*, 52 (2010) 1472.
16. A. Singh, Y. Lin, W. Liu, D. Kuanhai, J.Pan, B. Huang, C. Ren, D. Zeng, *J. Tai. Inst. Chem. E.*, 45 (2014) 1918.
17. A. Singh, I.Ahamad, V. K. Singh, M. A.Quraishi, *J. Solid State Electrochem.,* 15 (2011) 1087.
18. D. K. Yadav, M. A.Quraishi, *Ind. Eng. Chem. Res.*, 51 (2012) 14966.
19. K. F. Khaled, M. A. Amin, *Corros. Sci.*, 51 (2009) 1964.
20. A. Singh, Y. Lin, E. E. Ebenso, W. Liu, J. Pan, B. Huang, *J. Ind. Eng. Chem.*, 24 (2015) 219.
21. A.Khamis, M. M. Saleh, M. I. Awad, *Corros. Sci.,* 66 (2013) 343.
22. D. K. Yadav, D. S. Chauhan, I.Ahamad, M. A.Quraishi, *RSC Adv.*, 3 (2013) 632.
23. K. M. Ismail, *Electrochim.Acta,* 53 (2008) 5953.
24. A. Singh, Y. Lin, W. Liu, E. E. Ebenso, J. Pan, *Int. J. Electrochem. Sci.,* 8 (2013) 12884.
25. A. Singh, Yuanhua Lin, K. R. Ansari, M. A.Quraishi, E. E. Ebenso, Songsong Chen, W. Liu, *Appl. Surf. Sci.,*359 (2015) 331.
26. D. K. Yadav, M. A.Quraishi, B.Maiti, *Corros. Sci.,* 55 (2012) 254.
27. [Yuanhua Lin, Ambrish Singh, E. E. Ebenso, Yuanpeng Wu, Chunyang Zhu,H. Zhu,*J. Tai. Inst. Chem. Eng.*, 46 (2015) 214.
28. Ambrish Singh, Y. Lin, W. Liu, S. Yu, J. Pan, C. Ren, D. Kuanhai,*J. Ind. Eng. Chem.,* 20 (2014) 4276.
29. A. Singh, Y. Lin, M. A.Quraishi, O. L.Olasunkanmi, O. E.Fayemi, Y.Sasikumar, B.Ramaganthan, I. Bahadur, I. B. Obot, A. S.Adekunle, M. M.Kabanda, E. E. Ebenso, Molecules, (2015) 2015122.
30. K.R. Ansari, M.A. Quraishi, A. Singh, *Corros. Sci.*, 79 (2014) 5.
31. K.R. Ansari, M.A. Quraishi, A. Singh, *Corros. Sci.,* 95 (2015) 62.
32. Y. Lin, A. Singh, Eno E. Ebenso, M. A. Quraishi, Y. Zhou, Y. Huang, *Int. J. Electrochem. Sci.,*10 (2015) 194.

33. Ambrish Singh, Yuanhua Lin, Wanying Liu, Eno E. Ebenso, Jie Pan,*Int. J. Electrochem. Sci.,* 8 (2013) 12884.
34. A. Singh, Y. Lin, E.E. Ebenso, W. Liu, B. Huang,*Int. J. Electrochem. Sci.*, 9 (2014) 5993.
35. A. Singh, Y. Lin, Chunyang Zhu, Y. Wu, E. E. Ebenso, *Chin. J. Pol. Sci.,* 33 (2015) 339.
36. H.Keles, M.Keles, I.Dehri, O.Serindag, *Col. Surf. A,*320 (2008) 138.
37. F.Bentiss, C.Jama, B.Mernari, H. E.Attari, L. E.Kadi, M.Lebrini, M.Traisnel, M.Lagrenée, *Corros. Sci.,*51 (2009)1628.
38. Priyanka Singh, Ambrish Singh, M.A. Quraishi, *J. Taiwan Inst. Chem. E.*, 60 (2016) 588.
39. H. Ashassi-Sorkhabi, B. Shaabani, D. Seifzadeh, *Appl. Surf. Sci.*, 239 (2005) 154.
40. Xihua Xu, A. Singh, Z. Sun, K. R. Ansari, Y. Lin, *R. Soc. Open Sci.*, 4 (2017) http://dx.doi.org/10.1098/rsos.170933.
41. A. Singh, Y. Lin, I. B. Obot. E. E. Ebenso, *J. Mol. Liq.*, 219 (2016) 865.
42. A. Singh, I. Ahamad, M. A. Quraishi, *Arab. J. Chem.,* 9 (2016) S1584.
43. Ambrish Singh,Mohd Talha, Xihua Xu, Zhipeng Sun, Yuanhua Lin, *ACS Omega*, 2 (2017) 8177.
44. M. A. Quraishi, A. Singh, V. K. Singh, D. K. Yadav, A. K. Singh, *Mater. Chem. Phys.,* 122 (2010) 114.
45. Chitrasen Gupta, IshtiaqueAhamad, Ambrish Singh, Xihua Xu, Zhipeng Sun, Yuanhua Lin, *Int. J. Electrochem. Sci.,*12 (2017) 6379
46. B. M. Quinn, I. Prieto, S. K. Haram, A. J. Bard, *J. Phys. Chem. B*, 105 (2001) 7474.
47. Ambrish Singh, Y. Lin, I. B. Obot, E. E. Ebenso, K. R. Ansari, M. A. Quraishi, *Appl. Surf. Sci.*, 356 (2015) 341.
48. M.Tsionsky, A. J. Bard, D. Dini, F. Decker, *Chem, Mater.*, 10 (1998) 2120.
49. A.Maljusch, C.Senoz, M.Rohwerder, W.Schuhmann, *Electrochim.Acta*, 82 (2012) 339.
50. W. Liu, A. Singh, Y. Lin, E. E. Ebenso, G. Tianhan, C. Ren, *Int. J. Electrochem. Sci.*, 9 (2014) 5560.
51. K.R. Ansari, M.A. Quraishi, Ambrish Singh, *J. Ind. Eng. Chem.*, 25 (2015) 89.
52. K. R. Ansari, M. A. Quraishi, A. Singh, *J. Assoc. Arab Univ. Bas. Appl. Sci.*, (2015) http://dx.doi.org/10.1016/j.jaubas.2015.11.003.
53. I.B. Obot, S. Kaya, C. Kaya, B. Tüzün, *Physica E*, 80 (2016) 82.
54. A.Popova, M.Christov, T.Deligeorgiev, *Corrosion*, 59 (2003) 756.
55. E.E. Ebenso, T. Arslan, F. Kandemirli, N. Caner, I. Love, *Int. J. Quant. Chem.* 110 (2010) 1003.
56. S.K. Saha, A. Dutta, P. Ghosh, D. Sukul, P.Banerjee, *Phys. Chem. Chem. Phys.* 17 (2015) 5679.
57. A.Y. Musa, A.A.H. Kadhum, A.B. Mohamad, M.S.Takriff, *Mater. Chem. Phys.* 129 (2011) 660.